Applied Surface Science 724 (2026) 165642

Contents lists available at ScienceDirect

Applied Surface Science

journal homepage: www.elsevier.com/locate/apsusc

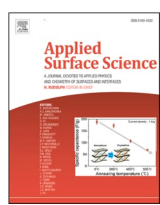

Full Length Article

Film and surface stress during Al_2O_3 and AlF_3 atomic layer deposition using *in situ* wafer curvature measurements

Ryan B. Vanfleet [a], Emanuele Sortino [b], Andrew S. Cavanagh [a], Victor M. Bright [b], Steven M. George [a,*]

[a] *Department of Chemistry, University of Colorado, Boulder, CO 80309, USA*
[b] *Department of Mechanical Engineering, University of Colorado, Boulder, CO 80309, USA*

A R T I C L E I N F O

Keywords:
Stress
Wafer curvature
Atomic layer deposition
Aluminum oxide
Aluminum fluoride

A B S T R A C T

In situ wafer curvature investigations were employed to measure film and surface stress during Al_2O_3 and AlF_3 atomic layer deposition (ALD). Isothermal *in situ* measurements can monitor intrinsic stress because they avoid the extrinsic stress resulting from thermal expansion coefficient mismatch between the film and substrate when conducting ex situ measurements at room temperature. The Al_2O_3 ALD films grown with trimethylaluminum (TMA) and H_2O had tensile film stress that decreased with temperature from ∼ 500 MPa at 125 °C to ∼ 100 MPa at 285 °C. The tensile stress was attributed to more hydrogen incorporation in the Al_2O_3 films at lower temperatures. In contrast, the AlF_3 ALD films grown with trimethylaluminum (TMA) and HF had no film stress. This lack of film stress was attributed to either the molecular nature of the AlF_3 films or the growth mechanism where TMA reacts with HF adsorbed on the AlF_3 surface. The *in situ* measurements could also observe the surface stress changes associated with the individual Al_2O_3 and AlF_3 ALD reactions. During Al_2O_3 ALD, the TMA reactions led to increasing compressive stress-thickness changes of −0.2 to −0.6 N/m from 125 °C to 285 °C, respectively. The H_2O reactions produced increasing tensile stress-thickness changes corresponding to the removal of the compressive stress-thickness changes. The compressive stress was attributed to repulsive interactions between the $AlCH_3$ surface species. During AlF_3 ALD, the TMA reactions also produced compressive stress-thickness changes of −0.4 N/m at 150 °C. The HF reactions then led to tensile stress-thickness changes corresponding to the removal of the compressive stress-thickness changes.

1. Introduction

Semiconductor and nanoelectromechanical (NEMS) devices have continued to shrink and are now at the nanometer scale. The effects of film stress on these devices has become more pronounced with continued miniaturization [1]. In addition, tensile stresses can cause film cracking [2]. Compressive stresses can also lead to film buckling, cracking and delamination [2]. For three dimensional or suspended structures with large surface-to-volume ratios, film stresses can also result in feature distortion and even collapse [3]. Understanding the stresses that arise during thin film deposition is important to combat stress-induced failure and to control potentially beneficial stresses [4].

Atomic layer deposition (ALD) is the premiere thin film deposition technique for ultrathin, conformal films [5]. ALD is characterized by sequential, self-limiting surface reactions that result in Angstrom-level thickness control and conformality even for extremely high aspect ratio [5,6]. Although ALD has already been adopted into many industrial fabrication processes, there is very little known about stresses during ALD film growth.

There have been previous *ex situ* studies of stress in ALD films. These measurements include investigations of Al_2O_3 [7–12], TiO_2 [13,14], ZrO_2 [15], and plasma-enhanced AlN ALD films [16,17]. These *ex situ* stress measurements of ALD films have been performed at room temperature and generally observe tensile stress. A portion of the tensile stress is attributed to thermal stress resulting from the temperature difference between the deposition temperature and room temperature.

Extrinsic stresses are stresses that are external to the film, such as the abovementioned thermal stress arising from thermal expansion mismatch between the film and substrate [1]. In contrast, intrinsic stresses are stresses related to film growth or film microstructure [1]. Differentiating between intrinsic stresses and extrinsic stresses is difficult in the presence of large coefficient of thermal expansion

* Corresponding author.
E-mail address: Steven.George@Colorado.edu (S.M. George).

https://doi.org/10.1016/j.apsusc.2025.165642
Received 12 July 2025; Received in revised form 12 December 2025; Accepted 18 December 2025
Available online 20 December 2025
0169-4332/© 2025 Elsevier B.V. All rights are reserved, including those for text and data mining, AI training, and similar technologies.

mismatches. In addition, *ex situ* stress measurements are unable to capture the surface stresses that result from different chemical species on the surface during individual ALD reactions. Surface stress cannot be monitored because the measurements are performed at the end of the ALD growth process.

In situ stress measurements allow for real-time monitoring of stress evolution during the film growth. Since the *in situ* measurements are performed at the deposition temperature, there are no thermal stresses. Additionally, *in situ* measurements can isolate surface stresses that can reveal the interactions between surface species during film growth. There have been no previous *in situ* stress measurements during ALD. There have been some *in situ* stress measurements during chemical vapor deposition (CVD) [18,19]. Surface stress has previously been measured during O_2 exposures on silicon surfaces [20,21]. Adsorbate-induced surface stress has also been monitored on Ni and Pt single crystals [22–25].

This study focuses on *in situ* stress measurements during Al_2O_3 ALD on silicon wafers. Al_2O_3 ALD is considered the model ALD system [26]. Al_2O_3 ALD uses trimethylaluminum (TMA) and water (H_2O) as reactants and proceeds according to [26–28]:

$$\text{(A) } AlOH^* + Al(CH_3)_3 \rightarrow AlOAl(CH_3)_2^* + CH_4 \tag{1}$$

$$\text{(B) } AlCH_3^* + H_2O \rightarrow AlOH^* + CH_4 \tag{2}$$

where the asterisk indicates the surface species. TMA reacts with surface hydroxyl groups ($AlOH^*$) and leaves the surface covered with methyl groups ($AlCH_3^*$). H_2O reacts with the $AlCH_3^*$ species and rehydroxylates the surface.

To probe the effects of a different co-reactant, additional measurements were performed during AlF_3 ALD using TMA and hydrogen fluoride (HF) as the reactants. This reaction proceeds according to [29]:

$$\text{(A) } AlF_3{:}HF^* + Al(CH_3)_3 \rightarrow AlF_3{:}AlF(CH_3)_2^* + CH_4 \tag{3}$$

$$\text{(B) } AlF_3{:}AlF(CH_3)_2^* + 3HF \rightarrow AlF_3{:}HF^* + 2CH_4 \tag{4}$$

Similar to the Al_2O_3 ALD reactions, the TMA reaction leaves the surface covered with $AlCH_3^*$ methyl species. HF then reacts with $AlCH_3^*$ species and forms AlF^* species. The similarities and differences between the Al_2O_3 and AlF_3 ALD reactions provide a comparison between surface reactions and stress in the respective films.

This study measured *in situ* stress during Al_2O_3 and AlF_3 ALD on silicon wafers using wafer curvature techniques. The Al_2O_3 ALD films exhibited tensile intrinsic residual stress at all deposition temperatures. The magnitude of the tensile stress decreased with increasing deposition temperature. In contrast, the AlF_3 ALD films exhibited no intrinsic residual stress. Surface stresses corresponding to the surface reactions were measured for both ALD processes. A compressive surface stress was observed after the TMA reactions and a release of this compressive surface stress was observed after reaction with either H_2O or HF.

2. Experimental methods

2.1. Wafer curvature technique

The *in situ* stress measurements were performed using wafer curvature techniques [30,31]. A thin substrate will bend in response to stress in the film on the substrate. The relative change in the position of spots in a laser beam array reflected off the substrate can be used to determine the substrate curvature. The Stoney equation relates the stress in the film to the curvature of the substrate [32].

$$\kappa = \frac{1}{R} = \frac{6\sigma_f t_f}{B_s\left(t_s^2\right)}$$

$$\sigma_f t_f = \frac{\kappa B_s\left(t_s^2\right)}{6} \tag{5}$$

κ is the curvature (1/m), R is the radius of curvature (m), B_s is the biaxial modulus of the substrate (Pa), t_s is the substrate thickness (m), t_f is the film thickness (m), and σ_f is the average stress in the film (Pa). The product $\sigma_f t_f$ is known as the stress-thickness. This stress-thickness can be calculated from the measured curvature and substrate properties without any prior knowledge about the deposited film.

The *in situ* curvature measurements were accomplished using a multibeam optical stress sensor (MOSS) [30] from k-space Associates. The MOSS instrument was set up in conjunction with a custom, hot wall, radial flow reactor as shown in Fig. 1. The silicon wafer used as a substrate lies horizontally on a platform as illustrated in Fig. 1a. The silicon wafer is only held in position by gravity. A carrier gas and the ALD reactants are introduced directly above the wafer and flow radially from the center to the edges as shown in Fig. 1b.

Film deposition can easily occur on the backside of the wafer under normal ALD conditions. If a film is deposited on both sides of the substrate, the stresses on one side cancel the stresses on the other side. Therefore, the ALD must be limited to the top side of the substrate for accurate curvature measurements. To stop backside deposition, a second stream of inert gas flows upwards from under the wafer and purges around the wafer edge to prevent reactants from reaching the backside of the wafer as depicted in Fig. 1b. The carrier gas flow on the frontside and the purge gas flow on the backside of the wafer are constant throughout the ALD process. Due to the radial flow design, the ALD reactions will saturate in the center of the wafer before the edges. However, the self-limiting nature of the ALD reactions leads to uniformity across the wafer after long reactant exposures.

2.2. Silicon wafers and curvature measurements

As illustrated in Fig. 1a, the laser beam array for the curvature measurement enters through a viewport at the bottom of the reactor and reflects off the backside of the wafer. The wafers were double-side polished, 200 μm thick silicon (100) wafers from Seigert Wafer. They were 76.2 mm in diameter and had a p-type resistivity between 1–20 Ω cm. These thinner-than-normal wafers result in a larger curvature for a given stress and produce a more sensitive measurement. Additionally, the wafers have no flats or notches for compatibility with the radially symmetric design of the reactor. Each wafer was cleaned and prepared for deposition by first flowing a low concentration of ozone over the wafer for 30 min at the deposition temperature. Nitrogen gas (UHP, 99.999 % purity, Airgas) heated to the deposition temperature was used for both the carrier gas and backside purge.

All curvature measurements were referenced to the curvature of the sample measured over a 5 min period at reaction conditions immediately prior to beginning film deposition. Curvature measurements were then recorded continuously throughout the ALD film growth at a rate of about 30 points per min. This measurement time is much shorter than the average ALD cycle time of 6.5 min. Each data point consists of the average of 16 laser beams in a 4 × 4 array reflecting from a 12 mm x 12 mm square area in the center of the wafer.

To validate the *in situ* curvature measurements, *in situ* measurements were directly compared with *ex situ* measurements on the same samples. Stress in Al_2O_3 films was measured under a variety of conditions. *Ex situ* measurements consisted of room temperature curvature measurements before and after the ALD process. These *ex situ* measurements were performed on a k-space MOS Ultrascan instrument housed at the National Institute for Standards & Technology (NIST) in Boulder, CO. Good agreement between the two measurements was observed after accounting for the thermal stress inherent in the *ex situ* measurements. This agreement established the validity of the *in situ* measurements.

2.3. ALD film growth

ALD was performed with a constant nitrogen flow of 180 sccm as the

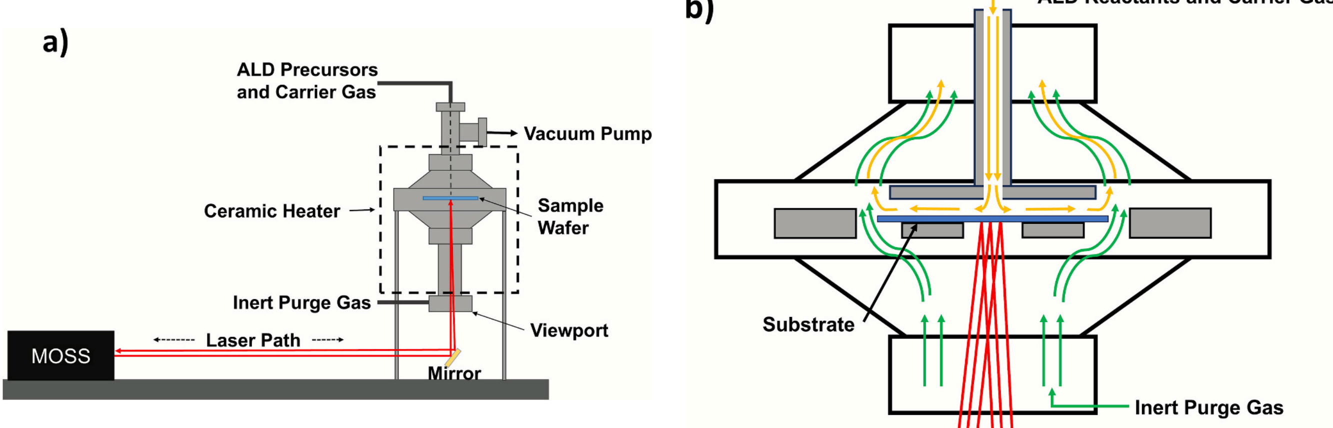

Fig. 1. (a) Side view of wafer curvature apparatus showing vacuum reactor containing wafer, multibeam optical stress sensor (MOSS), and laser path. (b) On frontside of the wafer, gas flows radially from the center to the edges. On the backside, gas flows around the wafer to prevent backside deposition.

top-side carrier gas and a constant nitrogen flow of 1000 sccm as the backside purge gas. The pressure differential from these nitrogen flows causes some curvature of the wafer. This pressure differential does not affect the measurements since the induced curvature is constant.

The Al_2O_3 ALD sequence consisted of 15 consecutive trimethylaluminum (TMA, 97 %, Sigma-Aldrich) mini-doses for 1 s. Multiple mini-dose sequences were used to minimize the pressure transients during precursor exposures. These smaller pressure transients were needed to eliminate backside deposition on the wafer during ALD. Each TMA mini-dose was followed by a 4 s purge. A 90 s purge followed the conclusion of the TMA mini-doses. Subsequently, there were 15 consecutive H_2O mini-doses for 1 s. Each H_2O mini-dose was followed by a 5 s purge. Another 90 s purge followed the conclusion of the H_2O mini-doses. Each TMA and H_2O mini-dose peaked at a partial pressure of ~ 0.1 Torr as measured by a Baratron® capacitance manometer on the gas manifold. Al_2O_3 ALD experiments were performed on the clean silicon wafers that were covered in a native silicon oxide with a nominal thickness of 1.8 nm.

The AlF_3 ALD sequence similarly consisted of 15 consecutive mini-doses of hydrogen fluoride (HF) for 1 s where each HF mini-dose was followed by an 8 s purge with a concluding 90 s purge. The HF mini-doses peaked at a partial pressure of ~ 0.25 Torr as measured by the Baratron® capacitance manometer on the gas manifold. Subsequently, there were 20 consecutive mini-doses of TMA for 1 s where each TMA mini-dose was followed by an 8 s purge with a concluding 90 s purge. AlF_3 ALD experiments were performed on wafers covered by 50 cycles of Al_2O_3 ALD.

The 15 consecutive mini-doses of precursor were determined to be adequate to reach saturation conditions across the wafer. Saturation was defined by a constant film growth over the entire wafer. Film thickness measurements at various positions across the wafer revealed that the film thicknesses were within 2 % of the average thickness. This uniform deposition occurred in the presence of the counterflow of N_2 inert gas purge on the backside of the wafer.

HF vapor for AlF_3 ALD was obtained from HF-pyridine (70 wt% HF, Sigma-Aldrich). HF-pyridine is a liquid at room temperature and is a safer option compared to anhydrous HF. The HF vapor in equilibrium above the HF-pyridine liquid has a vapor pressure of 90–100 Torr [33]. In contrast, the pyridine partial pressure is negligible [29]. HF abatement is performed by bubbling the reactor exhaust through an aqueous calcium oxide (CaO) solution. Excess HF is neutralized by the reaction of HF with CaO to form CaF_2.

Al_2O_3 ALD experiments were performed at temperatures between 125 °C and 285 °C with at least three and as many as 15 samples being measured at each temperature. Tabulated results showing temperatures, numbers of samples, mean values and error limits can be found in Tables S1 and S2 of the Supplementary Material. At 130 °C, each Al_2O_3 ALD cycle deposits an Al_2O_3 thickness of ~ 1.2 Å. Nominal film thicknesses deposited ranged from 10 nm to 30 nm. Thicknesses up to 100 nm were deposited for certain samples to determine if the stress changed for thicker films. AlF_3 ALD experiments were performed at 150 °C. Each AlF_3 ALD cycle deposits an AlF_3 thickness of ~ 1.0 Å. Film thicknesses were measured *ex situ* by variable-angle spectroscopic ellipsometry (M2000, JA Woolam). These spectroscopic ellipsometry measurements also confirmed that no film growth occurred on the backside of each wafer sample. Typical results are shown for all experiments.

3. Results and discussion

3.1. Al_2O_3 film stress

Fig. 2 shows the stress-thickness product, $\sigma_f t_f$, as a function of ALD cycles during Al_2O_3 ALD at 130 °C. There are two main features observed in the stress-thickness product. First, there is a more slowly varying change of the stress-thickness product versus ALD cycles that reveals the film stress. Second, there is rapid oscillatory change of the

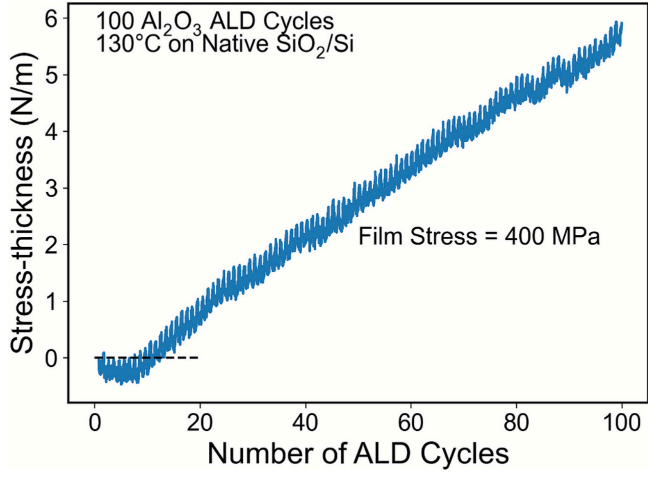

Fig. 2. Stress-thickness product versus number of ALD cycles during Al_2O_3 ALD on an ozone-cleaned silicon wafer at 130 °C. An initial compressive stress is indicated by negative values of the stress-thickness. Subsequent tensile stress of the film is shown by positive values of the stress-thickness. Constant positive slope indicates that amount of tensile stress is steady throughout film growth after the nucleation process.

stress-thickness product that coincides with each ALD cycle and is associated with surface stress.

During the first 10–15 ALD cycles, there is compressive stress as revealed by the negative values of the stress-thickness product. This initial compressive stress may result from the nucleation process that occurs during these ALD cycles. Once the film has reached the steady-state growth regime after about 5–10 ALD cycles, the stress becomes a constant tensile stress. This unchanging tensile stress results from the steady positive slope in Fig. 2. This tensile stress stays constant for the entire film growth for films up to 100 nm thick. The positive slope of the stress-thickness product in Fig. 2 is consistent with a stress of 400 MPa at 130 °C. By comparison, the critical tensile stress for the cracking of thicker Al_2O_3 ALD films is ~ 1000 MPa [2].

Fig. 3 shows the average film stress as a function of film thickness for the same results as in Fig. 2 at 130 °C. Film thickness was determined by measuring the total film thickness post-deposition and extrapolating to zero thickness at the start of the ALD growth. The average film stress was calculated by dividing the stress-thickness product by the film thickness. The average film stress again reveals the rapid oscillatory change that is synchronous with the ALD cycles.

The initial compressive stress is indicated by negative average film stress values. Subsequent tensile stress is revealed by positive average film stress values. Although the incremental stress becomes tensile after about 5 ALD cycles, the average film stress does not become tensile until about 12 ALD cycles. At this point, the film has a thickness just over 1 nm. The film does not reach its steady-state tensile stress value until the film is about 3 nm thick. Steady-state tensile stress must build up to overcome the effects of the initial compressive stress.

Fig. 4 shows the steady-state residual film stress for Al_2O_3 ALD films grown at different deposition temperatures. The error bars in Fig. 4 represent one standard deviation from the average stress measured at each temperature. The tensile residual stress in the Al_2O_3 ALD films decreases from 508 MPa at a deposition temperature of 125 °C to 113 MPa at a deposition temperature of 285 °C. This trend versus temperature is consistent with previous *ex situ* measurements for Al_2O_3 ALD film stress [12].

The *in situ* measured values of film stress are slightly lower than *ex situ* measured values of film stress for Al_2O_3 ALD films deposited at similar temperatures [12]. The *ex situ* measurements were performed at room temperature rather than the deposition temperature [12]. Under these conditions, the total stress measured is the combination of the residual film stress and the thermal stress. For an Al_2O_3 film on a silicon substrate, cooling the sample from the deposition temperature to room temperature will result in additional tensile stress. This additional

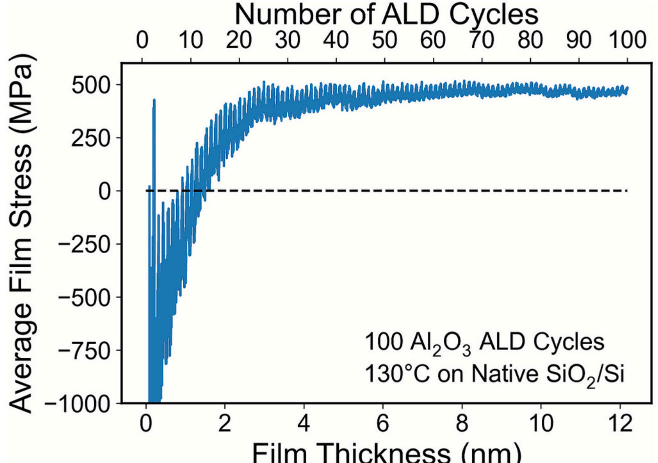

Fig. 3. Average film stress versus film thickness over 100 Al_2O_3 ALD cycles at 130 °C on an ozone-cleaned silicon wafer. Initial stress is compressive but becomes a constant tensile stress for thicknesses ≥ 3 nm.

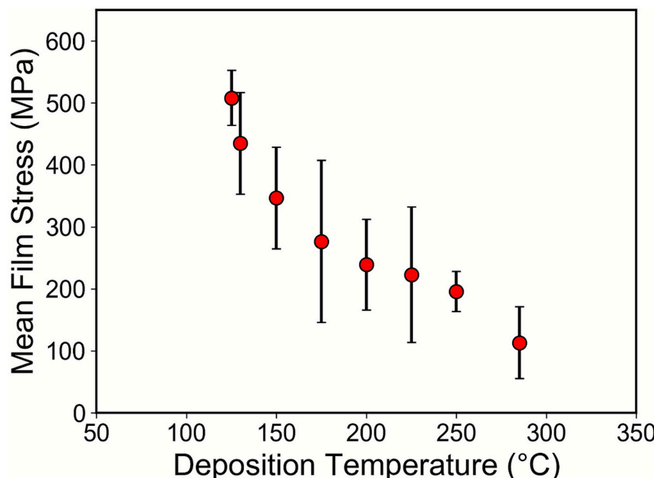

Fig. 4. Average steady-state film stress versus ALD temperature.

tensile stress occurs because Al_2O_3 has a larger coefficient of thermal expansion (CTE) than silicon [34].

In contrast, the *in situ* stress measurements do not include thermal stress. Consequently, the *in situ* stress measurements show lower tensile stress than the *ex situ* stress measurements. A comparison of the *in situ* measurements and the previous *ex situ* measurements [8–12,35,36] is shown in Fig. 5a. The differences are greater at higher deposition temperatures. The thermal stress inherent to the *ex situ* measurements can be estimated by Equation (6).

$$\sigma_{thermal} = \frac{E_f}{1-\nu_f}(\alpha_s - \alpha_f)\Delta T \tag{6}$$

Previously published values for the Al_2O_3 elastic modulus and Poisson ratio, as well as Al_2O_3 and silicon coefficients of thermal expansion are: $E_f = 170GPa$, $\nu_f = 0.24$, $\alpha_s = 3.45$ ppm/°C, $\alpha_f = 4.2$ ppm/°C [12,34]. In addition, ΔT is the difference between ambient temperature (assumed to be 20 °C) and the deposition temperature. Using these values, Equation (6) indicates that the ex situ stress measurements will overestimate the tensile stress by 18 MPa at 125 °C and 45 MPa at 285 °C. The *in situ* and *ex situ* film stress measurements are in close agreement when the thermal stress is taken into account.

The tensile stress in Al_2O_3 ALD films may result from hydrogen contained in the films. A significant amount of hydrogen in the form of O–H species is added to Al_2O_3 ALD films during deposition [37,38]. This hydrogen incorporation results in lower density Al_2O_3 ALD films [37]. The O–H species break the Al-O-Al network and may strain the surrounding Al-O bonds resulting in tensile stress. In similarity with the tensile stress in Al_2O_3 ALD films shown in Fig. 4, the hydrogen concentration decreases with increasing deposition temperature as displayed in Fig. 5b [37–40].

3.2. Al_2O_3 surface stress

Fig. 6 expands the stress-thickness plot versus time and shows the stress-thickness changes that occur during three Al_2O_3 ALD cycles at 200 °C (ALD cycles 33, 34 and 35). These stress-thickness changes are coincident with each group of 15 consecutive TMA and H_2O mini-doses. There are distinct oscillatory back-and-forth variations of the stress-thickness with each group of 15 consecutive TMA and H_2O mini-doses. The variations are interpreted as surface stress changes resulting from the different surface ligands present after the TMA and H_2O reactions. The saturation of the surface stress change occurs prior to the conclusion of 15 consecutive TMA and H_2O mini-doses for each surface reaction. This behavior indicates the saturation of the surface reactions.

Fig. 7 shows the relationship between the 15 consecutive TMA and

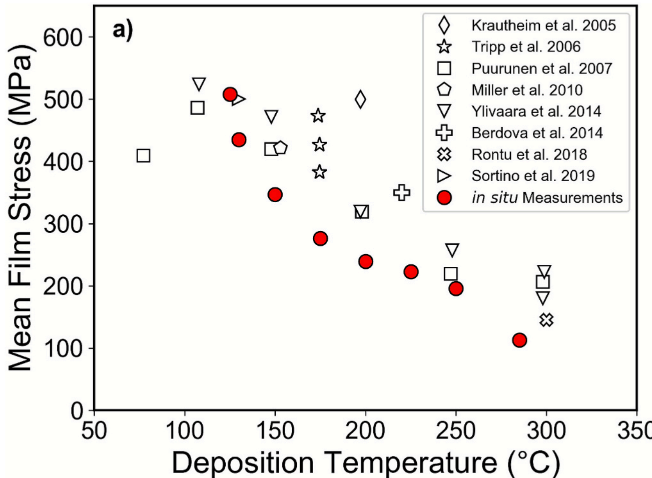

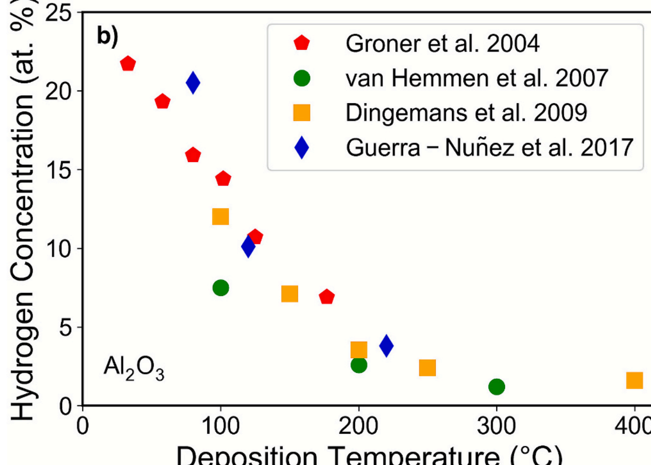

Fig. 5. (a) Ex situ average film stress measurements versus different deposition temperatures and *in situ* measurements from this work. (b) Hydrogen concentration in Al_2O_3 thermal ALD films as measured by elastic recoil detection analysis.

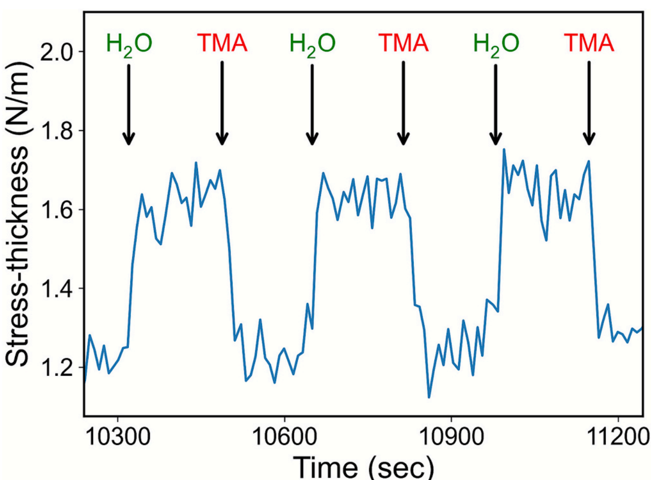

Fig. 6. Stress-thickness product during three Al_2O_3 ALD cycles at 200 °C. TMA reaction results in a compressive surface stress change and H_2O reaction yields a tensile (or release of compressive) surface stress change.

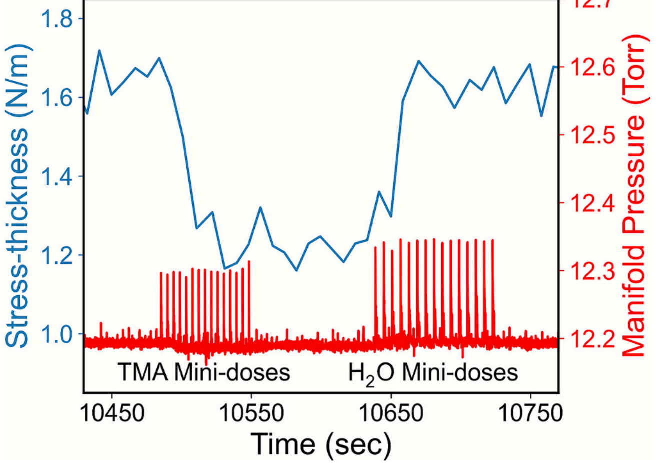

Fig. 7. Relationship between the 15 consecutive TMA and H_2O mini-doses during one Al_2O_3 ALD cycle at 200 °C and the stress-thickness product.

H_2O mini-doses and the stress-thickness for one Al_2O_3 ALD cycle at 200 °C. The manifold pressure is measured by a Baratron® capacitance manometer on the gas manifold. There is little change in the stress-thickness for the first 3 mini-doses. Subsequently, the change in the stress-thickness occurs over the next 3–4 mini-doses. Then the stress-thickness is constant for the remainder of the 15 mini-doses when the surface reaction has reached saturation. The negligible change in the stress-thickness for the first 3 mini-doses is believed to result from the precursors being consumed in the gas lines before they reach the wafer in the reactor.

The Al_2O_3 ALD reactions are illustrated in Fig. 8 [27]. TMA will react with surface hydroxyl groups and leave a surface covered with methyl ligands as displayed in Fig. 8a. Water vapor then reacts with the surface methyl ligands and replaces them with hydroxyl ligands as shown in Fig. 8b.

To explain the stress-thickness changes, the surface methyl groups may experience crowding and steric repulsion. This repulsion may produce the compressive surface stress observed in Fig. 6 and Fig. 7 during the TMA reaction. Similar compressive surface stress is observed during the formation of self-assembled monolayers (SAMs) of alkanethiols on gold surfaces [41,42]. This compressive stress is believed to result from the repulsive interactions between the neighboring alkanethiol chains.

The replacement of the surface methyl groups by OH species may relax the compressive stress and yield an effective tensile stress change. Alternatively, hydrogen bonding between surface hydroxyl groups may lead to the tensile stress observed in Fig. 6 during the H_2O reaction. The replacement of the surface hydroxyl groups by the methyl species may relax the tensile stress.

Fig. 9 shows the stress-thickness change as a function of Al_2O_3 ALD cycle number at 150 °C. Each point is obtained by averaging the stress-thickness change measurements during the purge step before and after each surface reaction and then taking the difference between the two averages. The stress-thicknesses changes are negative (compressive) during the TMA exposures. The stress-thickness changes are positive (tensile or release of compressive) during the H_2O exposures.

The initial Al_2O_3 ALD cycles in Fig. 9 show a transition period of about 20 cycles. During this time, the stress-thickness changes are smaller than the steady-state values observed between 40–150 ALD cycles. This transition period can be attributed to the nucleation of the Al_2O_3 film on the ozone-cleaned silicon wafer. The transition period could be dependent on the hydroxyl coverage on the initial ozone-cleaned surface.

After ozone cleaning of the initial silicon wafer, there is a native

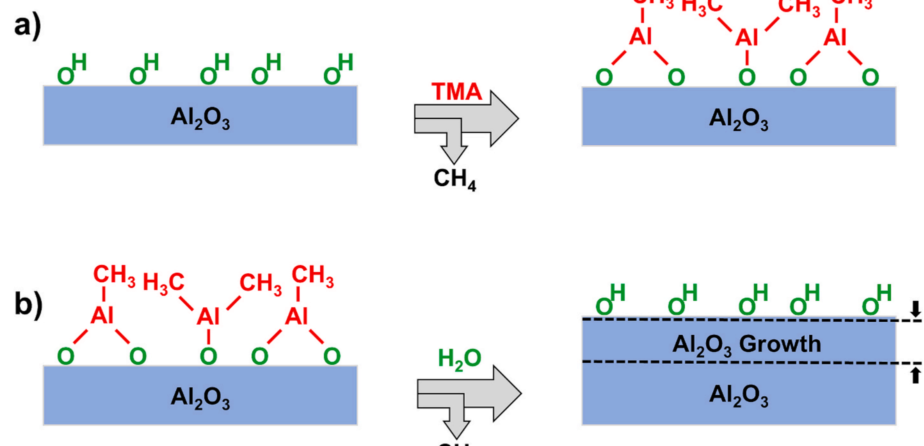

Fig. 8. Surface species during Al_2O_3 ALD. (a) TMA reaction leaves a surface covered with –CH_3 ligands. (b) H_2O reaction replaces the methyl ligands with hydroxyl groups.

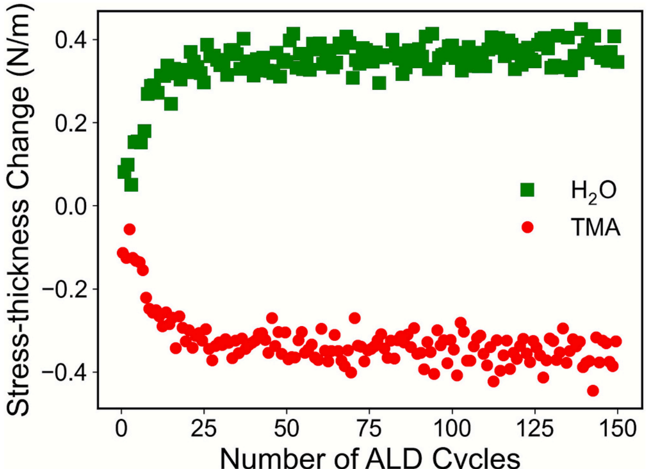

Fig. 9. Stress-thickness changes during Al_2O_3 ALD on an ozone-cleaned silicon wafer at 150 °C versus number of ALD cycles. Initial increase in the stress-thickness change corresponds to nucleation of the Al_2O_3 film.

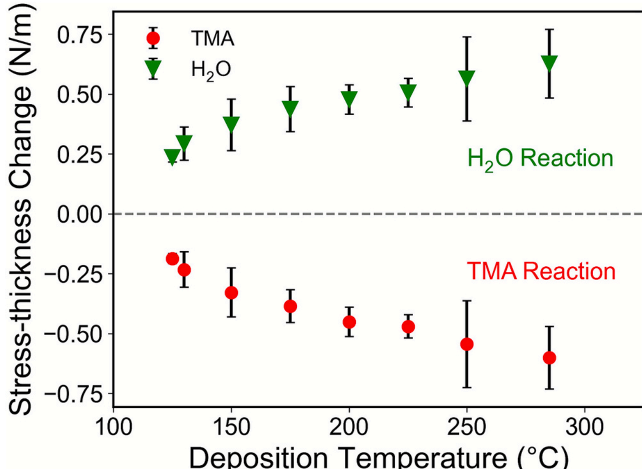

Fig. 10. Stress-thickness changes for Al_2O_3 ALD versus deposition temperatures.

oxide present. In addition, some hydroxyl groups are present that will facilitate the nucleation of the Al_2O_3 ALD film. More immediate nucleation of Al_2O_3 ALD on SiO_2 was reported in earlier studies [28,43]. These investigations employed silicon samples that were either oxidized *in situ* using a H_2O plasma, or were covered by SiO_2 films formed using SiO_2 plasma-enhanced CVD (PECVD) [28,43]. The rapid nucleation on these initial surfaces is attributed to a higher hydroxyl coverage than present on the ozone-cleaned silicon native oxide surface in these experiments.

The steady-state stress-thickness change also varies with the deposition temperature during Al_2O_3 ALD. Fig. 10 shows the stress-thickness changes as a function of deposition temperature for the H_2O and TMA reactions. The stress-thickness changes are approximately +/- 0.2 N/m at 125 °C. The stress-thickness changes are about +/- 0.6 N/m at 285 °C. The stress-thickness changes are larger at higher temperatures. This change in surface stress versus temperature is different than the change in film stress versus temperature shown in Fig. 4. The film stress is smaller at higher temperatures.

The temperature dependence of surface stress changes may help explain the origin of the surface stress. If the surface stress results from hydrogen bonding between hydroxyl groups, then the surface stress should decrease at lower hydroxyl coverages. Dehydroxylation of the Al_2O_3 surface occurs at higher deposition temperatures [27,44]. Dehydroxylation would lead to lower hydroxyl coverages and lower surface stress if the surface stress is caused by hydrogen bonding. However, the results in Fig. 10 display larger stress-thickness changes at higher temperatures.

The stress-thickness changes could also originate from repulsive interactions between methyl groups that lead to compressive stress. However, the absolute methyl coverage on Al_2O_3 surfaces is known to be lower at higher deposition temperatures [27]. This temperature dependence is apparently inconsistent with the stress-thickness change measurements in Fig. 10 that display larger changes at higher temperatures.

Although the methyl coverage is higher at lower temperatures, the change in surface stress may depend only on the change in methyl coverage. Even though there are more methyl groups at lower temperatures, the number of methyl groups that react at lower temperatures may be less than the number of methyl groups that react at higher temperatures. Previous studies have shown that water does not react with all the methyl groups on the methylated Al_2O_3 surface at low Al_2O_3 ALD temperatures [45]. At temperatures below 250 °C, water is not reactive enough to remove all the methyl groups and a significant amount of persistent methyl groups remain on the surface [45]. No surface stress change would be expected from the persistent methyl

groups.

Wafer curvature stress measurements only monitor changes in film and surface stress. Consequently, the stress-thickness changes observed in Fig. 10 result from differences in the surface ligand coverage. At low deposition temperatures, the change in the coverage of surface methyl ligands is lower because of the persistent methyl groups. At higher deposition temperatures, the surface reactions are more favorable and the change in surface methyl ligands is higher. Consequently, the surface stress changes are smaller at lower temperatures and larger at higher temperatures as observed in Fig. 10.

The water reaction with the surface methyl ligands becomes more favorable and the methyl ligands can be more fully removed at higher temperatures. This increased favorability of the water reaction with methyl groups also affects the Al_2O_3 ALD growth rate. One investigation has shown that the Al_2O_3 ALD growth per cycle progressively increases with temperature from 100 °C to 250 °C [45]. Other studies have reported that the Al_2O_3 ALD growth rate increases and then decreases slightly over this temperature range [28,37].

Al_2O_3 ALD processes using higher reactivity co-reactants such as O_2 plasma are able to more fully react with surface methyl groups at lower temperatures. These co-reactants produce larger changes in methyl coverage at lower temperatures [45]. These co-reactants could alter the temperature dependence for the stress-thickness changes shown in Fig. 10. If the surface methyl groups were able to be fully reacted and removed at all temperatures, then the measured stress-thickness changes would decrease with increasing temperature resulting from the declining number of methyl groups at higher temperatures.

3.3. AlF_3 film stress

Film stress in AlF_3 ALD films shows very different behavior compared with Al_2O_3 ALD films. The stress-thickness versus ALD cycle number for AlF_3 ALD at 150 °C on an Al_2O_3 ALD surface is displayed in Fig. 11. The first HF exposure causes a large compressive stress as the Al_2O_3 surface is fluorinated to form AlF_3. Since AlF_3 has a larger molar volume than ½ (Al_2O_3), the conversion from an oxide to a fluoride results in expansion and a compressive stress.

After the initial fluorination of the Al_2O_3 surface, the TMA and HF reactions result in oscillatory surface stress from the changing surface species. However, Fig. 11 reveals that there is no bulk film stress in the AlF_3 ALD film. The lack of film stress is signified by the zero slope of the stress-thickness plot. The AlF_3 films show no film stress even for much thicker films grown with up to 150 ALD cycles and thicknesses of 15 nm.

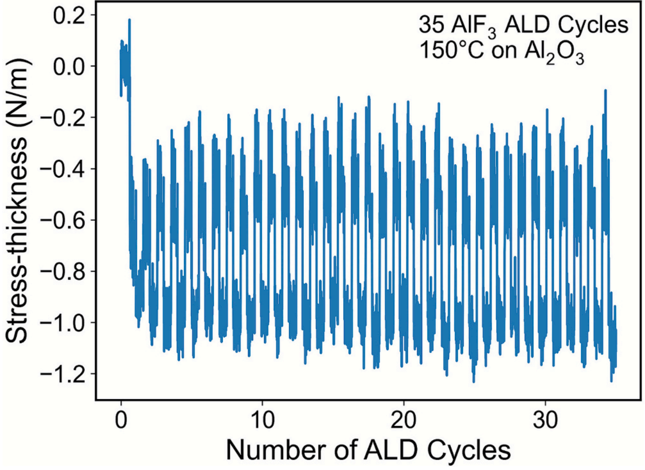

Fig. 11. Stress-thickness product during AlF_3 ALD at 150 °C. Initial compressive stress occurs during first HF exposure as underlying Al_2O_3 surface is fluorinated. Although surface reactions cause oscillatory stress-thickness values, there is no bulk stress in the AlF_3 film.

The lack of film stress in the AlF_3 ALD film may be attributed to the nature of AlF_3 as a molecular solid. The film is composed of AlF_3 units bonded together through Al-F-Al bridge bonds. These bridge bonds may be flexible and allow the AlF_3 units to rearrange within the film in response to any stress. The film is not constrained and no stress is locked into the film. In addition, the growth of AlF_3 ALD films is dependent on the reaction of TMA with adsorbed HF species on the AlF_3 surface [29]. Because the adsorbed HF species are not rigidly bound or constrained by the surface, there is very little stress transmitted to the underlying AlF_3 film when new AlF_3 species are formed during the TMA reaction.

The AlF_3 ALD films are also amorphous as previously confirmed by grazing-incidence x-ray diffraction (GI-XRD) measurements [29]. This amorphous nature may also play a role in the lack of stress in the AlF_3 ALD film. There is no long-range order that constrains the AlF_3 molecules into specific positions in the AlF_3 film.

3.4. AlF_3 surface stress

Fig. 12 shows an expansion of the stress-thickness results in Fig. 11 during three AlF_3 ALD cycles (ALD cycles 19, 20 and 21). The surface stress observed during AlF_3 ALD is very similar to the surface stress monitored during Al_2O_3 ALD. Fig. 12 shows that the TMA reaction leads to a negative surface stress change and is consistent with a compressive stress. In contrast, the HF reaction yields a positive surface stress change and is consistent with the release of the compressive stress. The surface stress changes are both at the same magnitude at ±0.5 N/m.

Fig. 13 shows the relationship between the 20 consecutive TMA and the 15 consecutive HF mini-doses and the stress-thickness measurements for one AlF_3 ALD cycle at 150 °C. The stress-thickness is altered almost immediately with the first HF and TMA mini-doses. Then the stress-thickness is constant for the remainder of the mini-doses when the surface reaction has reached saturation. The immediate change in the stress-thickness from the first mini-dose indicates that a smaller saturation exposure is necessary for the AlF_3 ALD chemistry than is required during the Al_2O_3 ALD chemistry. The transients in the stress-thickness signal during the HF mini-doses are coincident with the HF mini-doses. These transients are attributed to the higher HF mini-dose pressures causing the bending of the wafer sample during the HF mini-doses.

The surface ligands during AlF_3 ALD film growth are very similar to the surface ligands during Al_2O_3 ALD film growth. The TMA surface reaction given by Equation 3 leaves behind a surface covered with methyl ligands. The HF reaction given by Equation 4 removes the methyl ligands and replaces them with fluorine [29].

The surface methyl groups formed by the TMA surface reaction are

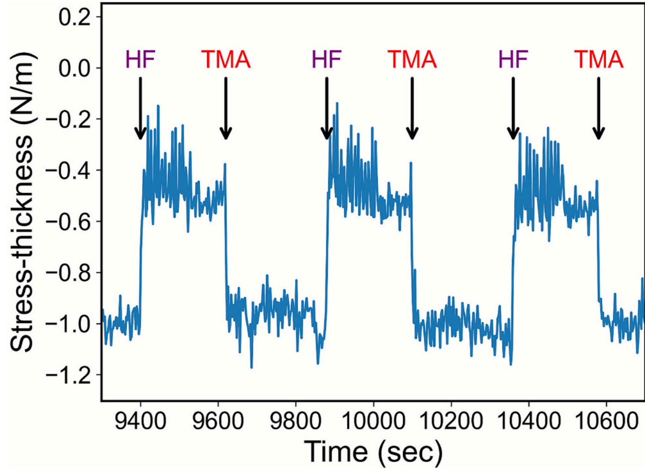

Fig. 12. Stress-thickness product during three AlF_3 ALD cycles at 150 °C. TMA reaction results in a compressive surface stress change and HF reaction yields a tensile (or release of compressive) surface stress change.

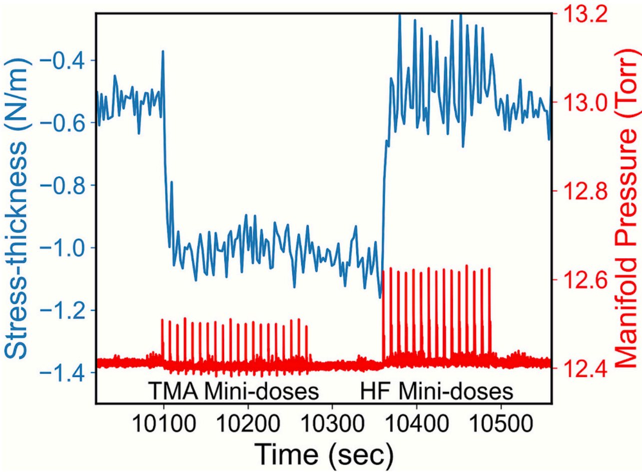

Fig. 13. Relationship between the 20 consecutive TMA and 15 consecutive HF mini-doses during one AlF_3 ALD cycle at 150 °C and the stress-thickness product.

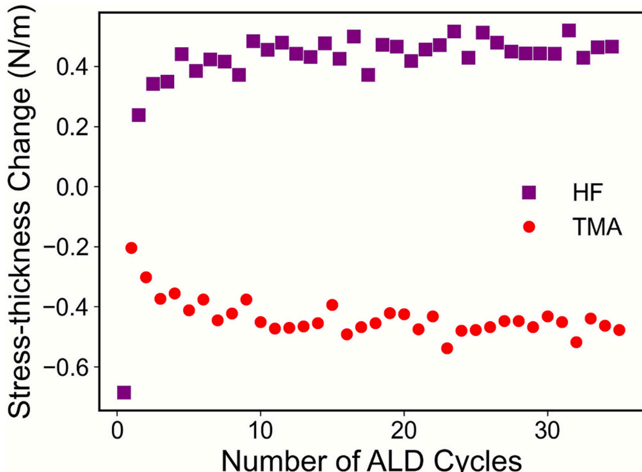

Fig. 14. Surface stress changes during AlF_3 ALD as a function of number of ALD cycles at 150 °C. First HF exposure shows very different behavior compared with subsequent HF reactions.

the commonality between Al_2O_3 ALD and AlF_3 ALD. Both TMA reactions lead to negative changes or compressive stress in the stress-thickness product. The similar effect of TMA during Al_2O_3 ALD and AlF_3 ALD is additional evidence that the surface methyl groups are the source of the compressive surface stress. Both the H_2O and HF co-reactants then remove the compressive surface stress by taking away the surface methyl groups during Al_2O_3 ALD and AlF_3 ALD, respectively.

Fig. 14 shows the stress-thickness changes for the HF and TMA reactions during AlF_3 ALD. About 5 ALD cycles are required for the AlF_3 ALD film to nucleate and for the stress-thickness change to become constant during each AlF_3 ALD cycle. The first HF exposure on the Al_2O_3 ALD surface results in a very different stress than the stress during subsequent HF exposures. This difference is attributed to the initial conversion of Al_2O_3 to AlF_3 as mentioned previously.

4. Conclusions

In situ stress measurements using the wafer curvature technique show that Al_2O_3 ALD films are under tensile stress during deposition at all temperatures. The magnitude of the tensile stress decreases from 508 MPa at a deposition temperature of 125 °C to around 113 MPa at a deposition temperature of 285 °C. The tensile stress may be caused by hydrogen incorporation into the film with less hydrogen incorporated at higher temperatures. AlF_3 ALD films show no film stress during deposition. Al-F-Al bridge bonds may be flexible enough to break and reform to not constrain the film and cause stress. The reaction between TMA and HF species on the surface may also proceed with little effect on the underlying AlF_3 film leading to negligible stress.

For both Al_2O_3 and AlF_3 ALD films, the TMA surface reaction leaves the surface covered with methyl groups. This methyl group coverage results in a compressive surface stress. The H_2O and HF surface reactions both eliminate surface methyl groups and remove the compressive surface stress for Al_2O_3 ALD and AlF_3 ALD, respectively. For Al_2O_3 ALD films, the magnitude of the stress-thickness change increases at higher deposition temperature. This larger change is attributed to more complete methyl group removal by the H_2O reaction at higher temperatures. Nucleation of the Al_2O_3 and AlF_3 ALD films can also be observed by the surface stress changes. The changes in surface stress during nucleation are smaller than the changes in surface stress during steady-state growth.

CRediT authorship contribution statement

Ryan B. Vanfleet: Writing – original draft, Methodology, Investigation, Formal analysis, Data curation. **Emanuele Sortino:** Writing – review & editing, Investigation, Formal analysis, Data curation. **Andrew S. Cavanagh:** Investigation. **Victor M. Bright:** Writing – review & editing, Supervision, Resources, Project administration, Methodology, Funding acquisition, Conceptualization. **Steven M. George:** Writing – review & editing, Supervision, Resources, Project administration, Methodology, Funding acquisition, Conceptualization.

Funding

This work was supported by Applied Materials; the Sierra Nevada Corporation; and the U.S. Army Research Laboratory and the U.S. Army Research Office [contract number W911NF-14-C-0007].

Declaration of competing interest

The authors declare the following financial interests/personal relationships which may be considered as potential competing interests: Ryan B. Vanfleet reports financial support was provided by Applied Materials Inc. Ryan B. Vanfleet, Emanuele Sortino, Andrew S. Cavanagh, Victor M. Bright and Steven M. George reports financial support was provided by Sierra Nevada Corporation. Victor M. Bright reports financial support was provided by US Army Research Office. If there are other authors, they declare that they have no known competing financial interests or personal relationships that could have appeared to influence the work reported in this paper.

Acknowledgements

The authors acknowledge useful discussions with Joseph Behnke at Applied Materials.

Appendix A. Supplementary data

Supplementary data to this article can be found online at https://doi.org/10.1016/j.apsusc.2025.165642.

Data availability

Data will be made available on request.

References

[1] G. Abadias, E. Chason, J. Keckes, M. Sebastiani, G.B. Thompson, E. Barthel, G. L. Doll, C.E. Murray, C.H. Stoessel, L. Martinu, Review article: stress in thin films and coatings: current status, challenges, and prospects, J. Vac. Sci. Technol. A 36 (2018) 020801, https://doi.org/10.1116/1.5011790.
[2] S.H. Jen, J.A. Bertrand, S.M. George, Critical tensile and compressive strains for cracking of Al_2O_3 films grown by atomic layer deposition, J. Appl. Phys. 109 (2011) 084305, https://doi.org/10.1063/1.3567912.
[3] N.T. Eigenfeld, J.M. Gray, J.J. Brown, G.D. Skidmore, S.M. George, V.M. Bright, Ultra-thin 3D nano-devices from atomic layer deposition on polyimide, Adv. Mater. 26 (2014) 3962, https://doi.org/10.1002/adma.201400410.
[4] M. Huff, Review paper: residual stresses in deposited thin-film material layers for micro- and nano-systems manufacturing, Micromachines 13 (2022) 2084, https://doi.org/10.3390/mi13122084.
[5] S.M. George, Atomic layer deposition: an overview, Chem. Rev. 110 (2010) 111, https://doi.org/10.1021/cr900056b.
[6] J.W. Elam, D. Routkevitch, P.P. Mardilovich, S.M. George, Conformal coating on ultrahigh-aspect-ratio nanopores of anodic alumina by atomic layer deposition, Chem. Mater. 15 (2003) 3507, https://doi.org/10.1021/cm0303080.
[7] M. Berdova, T. Ylitalo, I. Kassamakov, J. Heino, P.T. Törmä, L. Kilpi, H. Ronkainen, J. Koskinen, E. Hæggström, S. Franssila, Mechanical assessment of suspended ALD thin films by bulge and shaft-loading techniques, Acta Mater. 66 (2014) 370, https://doi.org/10.1016/j.actamat.2013.11.024.
[8] G. Krautheim, T. Hecht, S. Jakschik, U. Schröder, W. Zahn, Mechanical stress in ALD-Al_2O_3 films, Appl. Surf. Sci. 252 (2005) 200, https://doi.org/10.1016/j.apsusc.2005.01.118.
[9] D.C. Miller, R.R. Foster, S.H. Jen, J.A. Bertrand, S.J. Cunningham, A.S. Morris, Y. C. Lee, S.M. George, M.L. Dunn, Thermo-mechanical properties of alumina films created using the atomic layer deposition technique, Sens. Actuators, A 164 (2010) 58, https://doi.org/10.1016/j.sna.2010.09.018.
[10] V. Rontu, A. Nolvi, A. Hokkanen, E. Haeggström, I. Kassamakov, S. Franssila, Elastic and fracture properties of free-standing amorphous ALD Al_2O_3 thin films measured with bulge test, Mater. Res. Express 5 (2018) 046411, https://doi.org/10.1088/2053-1591/aabbd5.
[11] M.K. Tripp, C. Stampfer, D.C. Miller, T. Helbling, C.F. Hermann, C. Hierold, K. Gall, S.M. George, V.M. Bright, The mechanical properties of atomic layer deposited alumina for use in micro- and nano-electromechanical systems, Sens. Actuators, A 130 (2006) 419, https://doi.org/10.1016/j.sna.2006.01.029.
[12] O.M.E. Ylivaara, X.W. Liu, L. Kilpi, J. Lyytinen, D. Schneider, M. Laitinen, J. Julin, S. Ali, S. Sintonen, M. Berdova, E. Haimi, T. Sajavaara, H. Ronkainen, H. Lipsanen, J. Koskinen, S.P. Hannula, R.L. Puurunen, Aluminum oxide from trimethylaluminum and water by atomic layer deposition: the temperature dependence of residual stress, elastic modulus, hardness and adhesion, Thin Solid Films 552 (2014) 124, https://doi.org/10.1016/j.tsf.2013.11.112.
[13] Y.J. Huang, G. Pandraud, P.M. Sarro, Characterization of low temperature deposited atomic layer deposition TiO_2 for MEMS applications, J. Vac. Sci. Technol. A 31 (2013) 01a148, https://doi.org/10.1116/1.4772664.
[14] O.M.E. Ylivaara, A. Langner, X.W. Liu, D. Schneider, J. Julin, K. Arstila, S. Sintonen, S. Ali, H. Lipsanen, T. Sajavaara, S.P. Hannula, R.L. Puurunen, Mechanical and optical properties of As-grown and thermally annealed titanium dioxide from titanium tetrachloride and water by atomic layer deposition, Thin Solid Films 732 (2021) 138758, https://doi.org/10.1016/j.tsf.2021.138758.
[15] W. Weinreich, L. Wilde, J. Müller, J. Sundqvist, E. Erben, J. Heitmann, M. Lemberger, A.J. Bauer, Structural properties of As-deposited and annealed ZrO_2 influenced by atomic layer deposition, substrate, and doping, J. Vac. Sci. Technol. A 31 (2013) 01a119, https://doi.org/10.1116/1.4765047.
[16] S. Goerke, M. Ziegler, A. Ihring, J. Dellith, A. Undisz, M. Diegel, S. Anders, U. Huebner, M. Rettenmayr, H.G. Meyer, Atomic layer deposition of AlN for thin membranes using trimethylaluminum and H_2/N_2 Plasma, Appl. Surf. Sci. 338 (2015) 35, https://doi.org/10.1016/j.apsusc.2015.02.119.
[17] P. Sippola, A.P. Perros, O.M.E. Ylivaara, H. Ronkainen, J. Julin, X.W. Liu, T. Sajavaara, J. Etula, H. Lipsanen, R.L. Puurunen, Comparison of mechanical properties and composition of magnetron sputter and plasma enhanced atomic layer deposition aluminum nitride films, J. Vac. Sci. Technol. A 36 (2018) 051508, https://doi.org/10.1116/1.5038856.
[18] S. Hearne, E. Chason, J. Han, J.A. Floro, J. Figiel, J. Hunter, H. Amano, I.S. T. Tsong, Stress evolution during metalorganic chemical vapor deposition of GaN, Appl. Phys. Lett. 74 (1999) 356, https://doi.org/10.1063/1.123070.
[19] G.J. Leusink, T.G.M. Oosterlaken, G. Janssen, S. Radelaar, The evolution of growth stresses in chemical-vapor-deposited tungsten films studied by in-situ wafer curvature measurements, J. Appl. Phys. 74 (1993) 3899, https://doi.org/10.1063/1.354485.
[20] D. Flötotto, Z.M. Wang, L.P.H. Jeurgens, E.J. Mittemeijer, Evolution of surface stress during oxygen exposure of clean Si(111), Si(100), and amorphous Si surfaces, J. Appl. Phys. 115 (2014) 023501, https://doi.org/10.1063/1.4850936.
[21] D. Sander, H. Ibach, Experimental-determination of adsorbate-induced surface stress - oxygen on Si(111) and Si(100), Phys. Rev. B 43 (1991) 4263, https://doi.org/10.1103/PhysRevB.43.4263.
[22] A. Grossmann, W. Erley, H. Ibach, Adsorbate-induced surface stress - Co on Ni(100) and Ni(111), Surf. Sci. 313 (1994) 209, https://doi.org/10.1016/0039-6028(94)91168-1.
[23] A. Grossmann, W. Erley, H. Ibach, Adsorbate-induced surface stress measurements - a new method for monitoring in-situ surface-reactions, Surf. Rev. Lett. 2 (1995) 543, https://doi.org/10.1142/s0218625x95000492.
[24] A. Grossmann, W. Erley, H. Ibach, Adsorbate-induced surface stress and surface reconstruction - oxygen, sulfur and carbon on Ni(111), Surf. Sci. 337 (1995) 183, https://doi.org/10.1016/0039-6028(95)00615-x.
[25] Z. Tian, D. Sander, N.N. Negulyaev, V.S. Stepanyuk, J. Kirschner, H- and O-induced compressive surface stress on Pt(111): experiments and density functional theory calculations, Phys. Rev. B 81 (2010) 113407, https://doi.org/10.1103/PhysRevB.81.113407.
[26] R.L. Puurunen, Surface chemistry of atomic layer deposition: a case study for the trimethylaluminum/water process, J. Appl. Phys. 97 (2005) 121301, https://doi.org/10.1063/1.1940727.
[27] A.C. Dillon, A.W. Ott, J.D. Way, S.M. George, Surface-chemistry of Al_2O_3 deposition using $Al(CH_3)_3$ and H_2O in a binary reaction sequence, Surf. Sci. 322 (1995) 230, https://doi.org/10.1016/0039-6028(95)90033-0.
[28] A.W. Ott, J.W. Klaus, J.M. Johnson, S.M. George, Al_2O_3 thin film growth on Si(100) using binary reaction sequence chemistry, Thin Solid Films 292 (1997) 135, https://doi.org/10.1016/s0040-6090(96)08934-1.
[29] Y. Lee, J.W. DuMont, A.S. Cavanagh, S.M. George, Atomic layer deposition of AlF_3 using trimethylaluminum and hydrogen fluoride, J. Phys. Chem. C 119 (2015) 14185, https://doi.org/10.1021/acs.jpcc.5b02625.
[30] E. Chason, P.R. Guduru, Tutorial: understanding residual stress in polycrystalline thin films through real-time measurements and physical models, J. Appl. Phys. 119 (2016) 191101, https://doi.org/10.1063/1.4949263.
[31] E. Chason, B.W. Sheldon, Monitoring stress in thin films during processing, Surf. Eng. 19 (2003) 387, https://doi.org/10.1179/026708403225010118.
[32] G. Janssen, M.M. Abdalla, F. van Keulen, B.R. Pujada, B. van Venrooy, Celebrating the 100th Anniversary of the Stoney equation for film stress: developments from polycrystalline steel strips to single crystal silicon wafers, Thin Solid Films 517 (2009) 1858, https://doi.org/10.1016/j.tsf.2008.07.014.
[33] Y. Lee, J.W. DuMont, S.M. George, Atomic layer etching of HfO_2 using sequential, self-limiting thermal reactions with $Sn(acac)_2$ and HF, ECS J. Solid State Sci. Technol. 4 (2015) N5013, https://doi.org/10.1149/2.0041506jss.
[34] O.M.E. Ylivaara, A. Langner, S. Ek, J. Malm, J. Julin, M. Laitinen, S. Ali, S. Sintonen, H. Lipsanen, T. Sajavaara, R.L. Puurunen, Thermomechanical properties of aluminum oxide thin films made by atomic layer deposition, J. Vac. Sci. Technol. A 40 (2022) 062414, https://doi.org/10.1116/6.0002095.
[35] R.L. Puurunen, J. Saarilahti, H. Kattelus, Implementing ALD layers in MEMS processing, ECS Trans. 11 (2007) 3, https://doi.org/10.1149/1.2779063.
[36] E. Sortino, J. P. Houlton, J. C. Gertsch, O. D. Supekar, G. D. Skidmore, S. M. George, C. T. Rogers and V. M. Bright. "Effect of Atomic Layer Etching on Residual Stress of Al_2O_3 ALD Ultra-Thin Film Suspended Structures". In *2019 20th International Conference on Solid-State Sensors, Actuators and Microsystems & Eurosensors XXXIII (TRANSDUCERS & EUROSENSORS XXXIII)*. 2019. 2404.
[37] M.D. Groner, F.H. Fabreguette, J.W. Elam, S.M. George, Low-Temperature Al_2O_3 atomic layer deposition, Chem. Mater. 16 (2004) 639, https://doi.org/10.1021/cm0304546.
[38] C. Guerra-Nunez, M. Döbeli, J. Michler, I. Utke, Reaction and growth mechanisms in Al_2O- deposited via atomic layer deposition: elucidating the hydrogen source, Chem. Mater. 29 (2017) 8690, https://doi.org/10.1021/acs.chemmater.7b02759.
[39] G. Dingemans, M.C.M. van de Sanden, W.M.M. Kessels, Influence of the deposition temperature on the c-Si surface passivation by Al_2O_3 films synthesized by ALD and PECVD, Electrochem. Solid-State Lett. 13 (2010) H76, https://doi.org/10.1149/1.3276040.
[40] J.L. van Hemmen, S.B.S. Heil, J.H. Klootwijk, F. Roozeboom, C.J. Hodson, M.C. M. van de Sanden, W.M.M. Kessels, Plasma and thermal ALD of Al_2O_3 in a Commercial 200 mm ALD Reactor, J. Electrochem. Soc. 154 (2007) G165, https://doi.org/10.1149/1.2737629.
[41] R. Berger, E. Delamarche, H.P. Lang, C. Gerber, J.K. Gimzewski, E. Meyer, H. J. Guntherodt, Surface stress in the Self-Assembly of Alkanethiols on Gold, Science 276 (1997) 2021, https://doi.org/10.1126/science.276.5321.2021.
[42] P. Shrotriya, K.K.S. Karuppiah, R. Zhang, A. Chandra, S. Sundararajan, Surface stress generation during formation of alkanethiol self-assembled monolayer (SAM), Mech. Res. Commun. 35 (2008) 43, https://doi.org/10.1016/j.mechrescom.2007.09.007.
[43] V. Vandalon, W.M.M. Kessels, Initial growth study of atomic-layer deposition of Al_2O_3 by vibrational sum-frequency generation, Langmuir 35 (2019) 10374, https://doi.org/10.1021/acs.langmuir.9b01600.
[44] V. Vandalon, W.M.M. Kessels, Revisiting the Growth Mechanism of Atomic Layer Deposition of Al_2O_3: a Vibrational Sum-Frequency Generation Study, J. Vac. Sci. Technol. A 35 (2017) 05c313, https://doi.org/10.1116/1.4993597.
[45] V. Vandalon, W.M.M. Kessels, What is limiting low-temperature atomic layer deposition of Al_2O_3? A vibrational sum-frequency generation study, Appl. Phys. Lett. 108 (2016) 011607, https://doi.org/10.1063/1.4939654.